Journal of Alloys and Compounds 750 (2018) 696–705

Contents lists available at ScienceDirect

Journal of Alloys and Compounds

journal homepage: http://www.elsevier.com/locate/jalcom

Influence of extrusion temperature on microstructure and mechanical behavior of duplex Mg-Li-Al-Sr alloy

Yan Yang [a, b, d, *], Xiaoming Xiong [a], Junfei Su [a], Xiaodong Peng [a, b], Haiming Wen [c, **], Guobing Wei [a], Fusheng Pan [a, b], Enrique J. Lavernia [d]

[a] School of Materials Science and Engineering, Chongqing University, Chongqing, 400044, China
[b] National Engineering Research Center for Magnesium Alloys, Chongqing University, Chongqing, 400044, China
[c] Department of Materials Science and Engineering, Missouri University of Science and Technology, Rolla, MO 65409, USA
[d] Department of Chemical Engineering and Materials Science, University of California, Irvine, CA 92697, USA

ARTICLE INFO

Article history:
Received 14 November 2017
Received in revised form
24 March 2018
Accepted 26 March 2018
Available online 27 March 2018

Keywords:
Mg-Li alloy
Extrusion temperature
Microstructure
Mechanical properties
Dynamic recrystallization

ABSTRACT

In this study, as-cast alloy Mg-9Li-3Al-2.5Sr (LAJ932) ingots were extruded at different temperatures using an extrusion ratio of 28, and the underlying microstructural evolution and mechanical behavior were investigated. The results show that grains in the extruded LAJ932 alloy are much finer than those in the as-cast one, which indicates that the microstructural evolution during extrusion is governed by dynamic recrystallization. With increasing extrusion temperature, the grain size of the extruded alloy increases, and the strength decreases whereas the elongation increases. The alloy extruded at 250 °C possesses the highest strength of 238 MPa with an elongation of 18.1%, whereas[1] the alloy extruded at 350 °C has the largest elongation of 21.6% with a strength of 208 MPa. The differences in microstructure characteristics between the α-Mg phase and β-Li phase in the alloy extruded at 250 °C suggest that continuous dynamic recrystallization (CDRX) occurs in the α-Mg phase during extrusion whereas the microstructure evolution in β-Li phase is governed by discontinuous dynamic recrystallization (DDRX). DDRX occurs in α-Mg phase to some extent and the fraction of DDRX grains in the alloys increases with increasing extrusion temperature.

1. Introduction

Magnesium alloys are scientifically and technologically relevant, partly due to their low density and attractive combination of physical and mechanical attributes [1,2]. Mg-Li alloys are of particular interest because they are considered to be amongst the lightest metallic structural materials known [3–5]. Ultralight Mg-Li alloys are being studied for application in the defense, electrical and aerospace industries where their combination of properties and density provide immediate benefits [6–8]. According to the Mg-Li phase diagram [9], the Li content in Mg-Li alloys critically influence both the microstructure and mechanical response of the alloys. For example, when Li < 5.7 wt%, Mg-Li is comprised of a single α-Mg phase, which is a Mg-rich solid solution with hcp structure formed by Li dissolved in Mg. In contrast, when the Li content is between 5.7 and 11 wt%, a α-Mg (hcp) + β-Li (bcc) duplex structure is formed, where β-Li phase is a Li rich solid solution with a bcc structure formed by Mg dissolution in Li. When the Li content is > 11 wt%, the corresponding alloy consists solely of the β-Li phase [10,11].

Mg-Li alloys with duplex structures possess favorable mechanical properties and therefore are potentially attractive for various applications. Plastic deformation is an effective way to improve the microstructure and thereby enhance the mechanical properties of Mg-Li alloys. For example, it has been reported that Mg-Li alloys can be further strengthened by plastic deformation methods such as extrusion, rolling and forging, etc. [12–15]. In related studies, Zhang et al. [16] reported that the tensile properties of Mg-Li-Zn-Gd alloys were improved significantly by extrusion due to the grain refinement and the presence of cracked I-phase particles. Furthermore, Dong et al. [17] studied a duplex Mg-5Li-2Zn alloy and reported that strength increased whereas the ductility tended

* Corresponding author. School of Materials Science and Engineering, Chongqing University, Chongqing, 400044, China.
** Corresponding author. Department of Materials Sciecne and Engineering, Missouri University of Science and Technology, Rolla, USA
E-mail addresses: yanyang@cqu.edu.cn (Y. Yang), wenha@mst.edu (H. Wen).

https://doi.org/10.1016/j.jallcom.2018.03.319
0925-8388/

to decrease with increasing extrusion ratio.

Interestingly, review of the published literature shows that our current understanding of the mechanisms that govern the influence of extrusion parameters (particularly the extrusion temperature) on the microstructure and mechanical behavior of duplex Mg-Li alloys remains inadequate. In particular, the influence of extrusion temperature on the microstructure evolution of different phases in duplex Mg-Li alloys has not been reported yet. In our previous study we reported that adding 2.5 wt% Sr into Mg-9Li-3Al alloy improves the strength of Mg-9Li-3Al-2.5Sr (LAJ932) [18,19]. On the basis of this lack of information, and based on our previous work, the objective of this study was to investigate the influence of extrusion temperature on microstructure evolution and mechanical behavior in a duplex structured Mg-Li-Al-Sr alloy (i.e., LAJ932).

2. Experimental procedures

The target alloy composition used in this study, LAJ932 was prepared using pure Mg (99.9 wt%), Li (99.9 wt%), Al (99.9 wt%) and a Mg-8Sr master alloy (Mg 92 wt%, Sr 8 wt%) as raw materials. The individual alloy constituents were mixed using the appropriate ratios and were melted in a melting furnace under the protection of a SF_6/CO_2 gas mixture. Then, the melt was cast in a $\Phi 90 \times 300$ mm permanent mold to prepare as-cast alloy ingots. The chemical composition of the test alloy was measured using a Hitachi Z-8000 atomic absorption spectrophotometer, and the results indicated that the alloy contained 8.56 wt% Li, 3.12 wt% Al and 2.47 wt% Sr with the balance Mg. The as-cast specimens were machined from Φ90 mm to Φ80 mm and homogenizing treatment was performed on them at 250, 300 and 350 °C respectively for 2 h in a vacuum furnace before extrusion. The homogenized specimens were extruded at 250, 300 and 350 °C respectively from Φ80 mm to Φ15 mm rods with an extrusion ratio of 28.

The microstructure of as-cast and extruded LAJ932 alloys was studied via optical microscopy (OM), scanning electron microscopy (SEM) and transmission electron microscopy (TEM). The OM and SEM samples were prepared following standard metallography sample preparation procedures. 2 vol% HNO_3 alcohol solution was used as the etchant. The OM investigations were carried out on a MDS optical microscope, and the SEM observations were performed on FEI XL30-SFEG microscope operated at 5 kV. The microstructure of the extruded alloys was observed in detail using TEM. The TEM and scanning transmission electron microscopy (STEM) imaging was performed on a JEOL 2500SE TEM/STEM or a CM 12 microscope operated at 200 or 120 kV, respectively. The TEM specimens were prepared by mechanical thinning followed by Ar ion milling. The ultrafine grain sizes of test alloys were measured on the TEM images using an Olympus analySIS FIVE software. For each sample, more than 200 grains were measured to calculate the average grain size. Phase composition in the as-cast LAJ932 alloy was obtained from the statistical analysis of more than 30 OM images using Image-Pro Plus software. Specimens for tensile tests with gauge size of $30 \times \Phi 6$ mm were machined from the central regions of the extruded samples along the extrusion direction and tensile tests were performed on a CMT-5105 tensile tester machine.

Finite element simulation was performed to study the deformation behavior of LAJ932 alloys during the extrusion using Deform-3D software. In this work, the friction coefficient was set to be 0.7 as an empirical parameter during hot extrusion [20]. Similarly, the billet was assumed to undergo elastic-plastic deformation whereas the die and plunger were assumed to be rigid and experienced no deformation during extrusion. A mesh structure with 5024 nodes and 5229 surface polygons for the billet was established. The billet was set to be extruded with an extrusion ratio of 28 during the simulation. The distribution of effective strain and stress during the extrusion was simulated and used in the discussion of our results.

3. Results

3.1. Microstructure of as-cast and extruded LAJ932 alloys

Fig. 1 shows the microstructure of as-cast Φ90 mm LAJ932 alloy ingot. Our previous research indicated that LAJ932 alloys contain: hcp α-Mg, bcc β-Li and intermetallic Al_4Sr phases [18,19]. Accordingly, the white area in Fig. 1(a) and the dark areas in Fig. 1(b) can be identified as the α-Mg phase whereas the grey areas correspond to eutectic structure containing both eutectic α-Mg and β-Li phases. The volume fraction of α-Mg phase is ~35.5% based on the statistics of more than 30 OM images using Image-Pro Plus software. The grain size of the primary α-Mg grains is ~130 μm whereas the grain size of eutectic α-Mg is ~5 μm. The bright phase in the eutectic area is the β-Li phase. The fraction of β-Li phase in the eutectic area is significantly higher than that of α-Mg phase. The white continuous "fish-bone" like intermetallic phase is Al_4Sr.

Fig. 2 displays OM micrographs of as-extruded LAJ932 alloys rods using different extrusion temperatures, with the extrusion direction indicated. The extruded alloys still consist of α-Mg, β-Li and Al_4Sr phases. However, the grains in the extruded alloys are much finer than those in the as-cast alloy. There are evident differences in the microstructure characteristics between the α-Mg and β-Li phases in the extruded alloy. Most of the α-Mg phase is elongated along the extrusion direction while β-Li phase exhibits equiaxed grains. The grains in the extruded alloys are composed of fine grains and ultrafine grains. The average size of primary α-Mg phase is ~12 μm while the value reaches to 16 and ~23 μm as temperature increases to 300 and 350 °C, respectively. The average size of fine grains of the β-Li phase in the alloy extruded at 250 °C is ~2 μm, whereas the corresponding values increase to ~4 and ~5 μm with the extrusion temperature increasing to 300 and 350 °C, respectively. The original continuously distributed Al_4Sr phase in the as-cast alloy was fractured during extrusion and the distribution of Al_4Sr phase in the extruded alloys is improved significantly after extrusion. Fig. 2 indicates that approximately equiaxed Al_4Sr particles with a size of ~2–15 μm are nearly homogeneously distributed in the extruded alloy. Extrusion temperature has no significant influence on the size and distribution of Al_4Sr phase due to its high-temperature stability [18].

TEM studies were carried out to study the ultrafine grains in the extruded alloy. TEM micrographs of as-extruded LAJ932 alloy with different extrusion temperatures are shown in Figs. 3–5, respectively. There are two types of grains evident in the TEM micrographs: the grain boundaries of the first type grains are irregular and the dislocation density in the grain interiors is relatively high, which is typical characteristics of continuous dynamic recrystallization (CDRX) grains [21], whereas the grain boundaries of the other type of grains are sharp with few dislocations inside the grains, which are typical attributes of discontinuous dynamic recrystallization (DDRX) grains. The grain size distributions of the ultrafine CDRX grains and DDRX grains in LAJ932 alloy extruded at different temperatures are shown in Figs. 3(c) (d), 4(c) (d) and 5(c) (d) respectively. Most DDRX grains fall in the range of 100–300 nm while CDRX grains are distributed in 100–500 nm when the extrusion temperature is 250 °C. When the extrusion temperature is increased to 300 °C, most DDRX grains have grain sizes of 200–400 nm whereas most of the CDRX grains are 100–700 nm in size. When the extrusion temperature reaches 350 °C, the sizes of most DDRX grains fall in 100–600 nm with those of CDRX grains

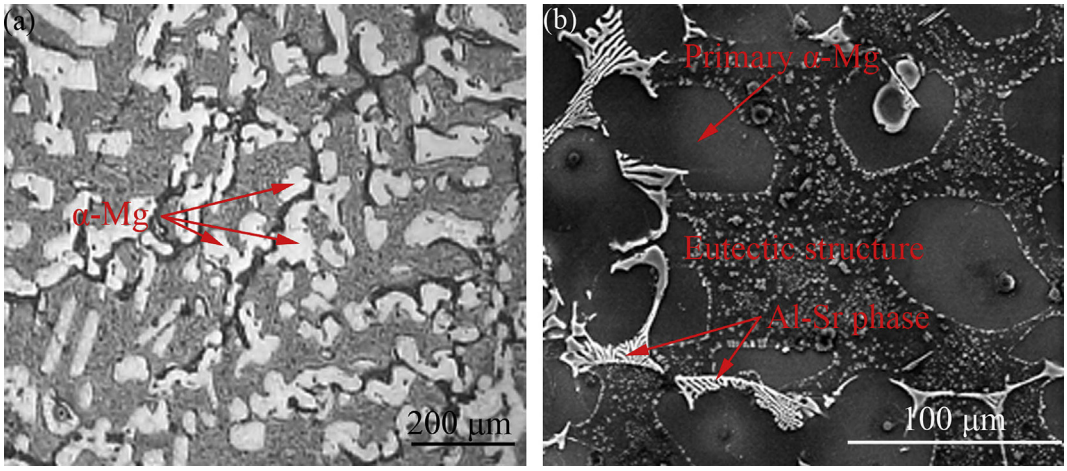

Fig. 1. Microstructure of as-cast Φ90 mm LAJ932 alloy ingot: (a) OM image (b) SEM image.

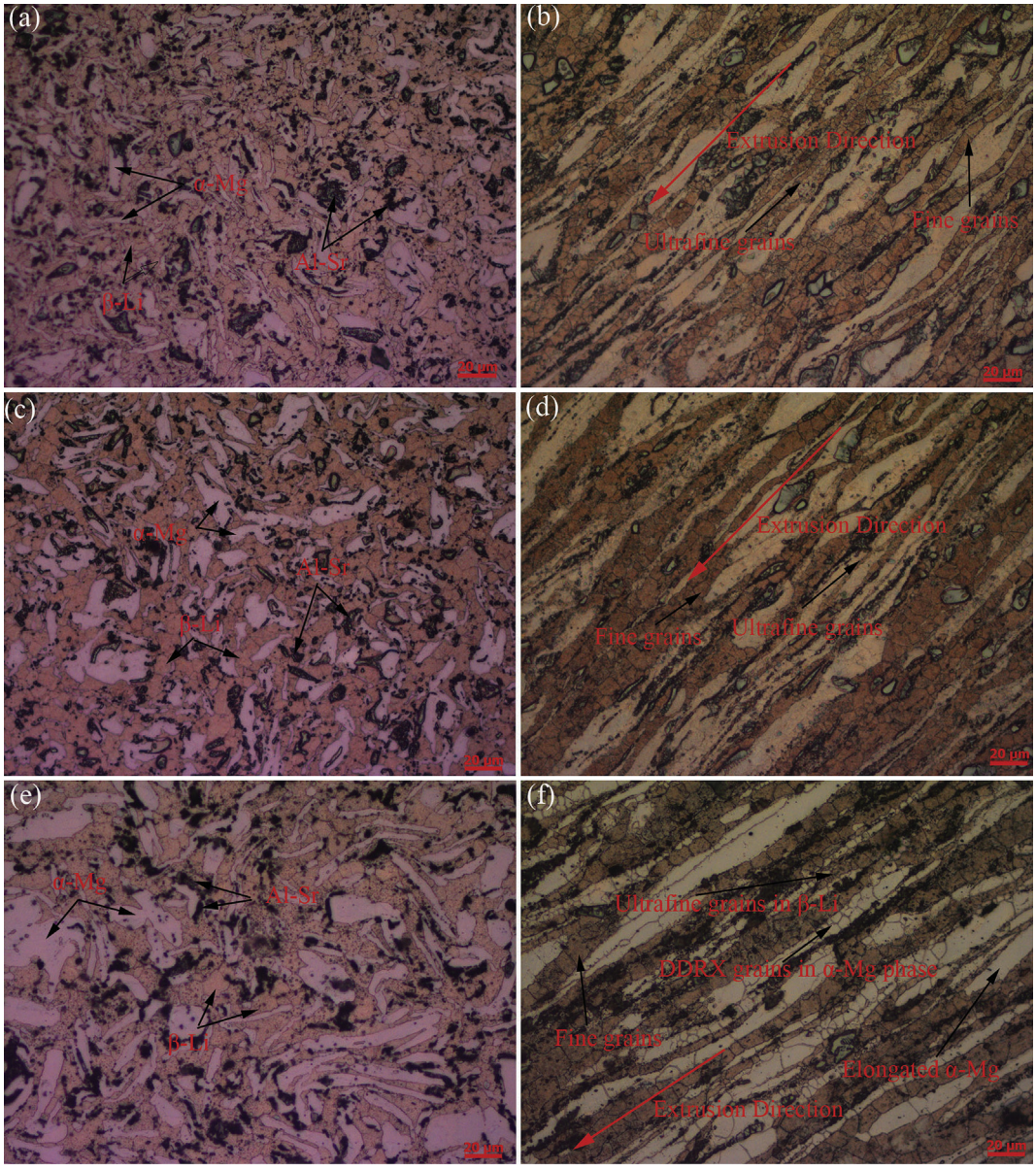

Fig. 2. OM micrographs of extruded LAJ932 alloy with different extrusion temperatures: (a) (b) 250 °C; (c) (d) 300 °C; (e) (f) 350 °C ((a) (c) (e): vertical to the extrusion direction, (b) (d) (f): along the extrusion direction).

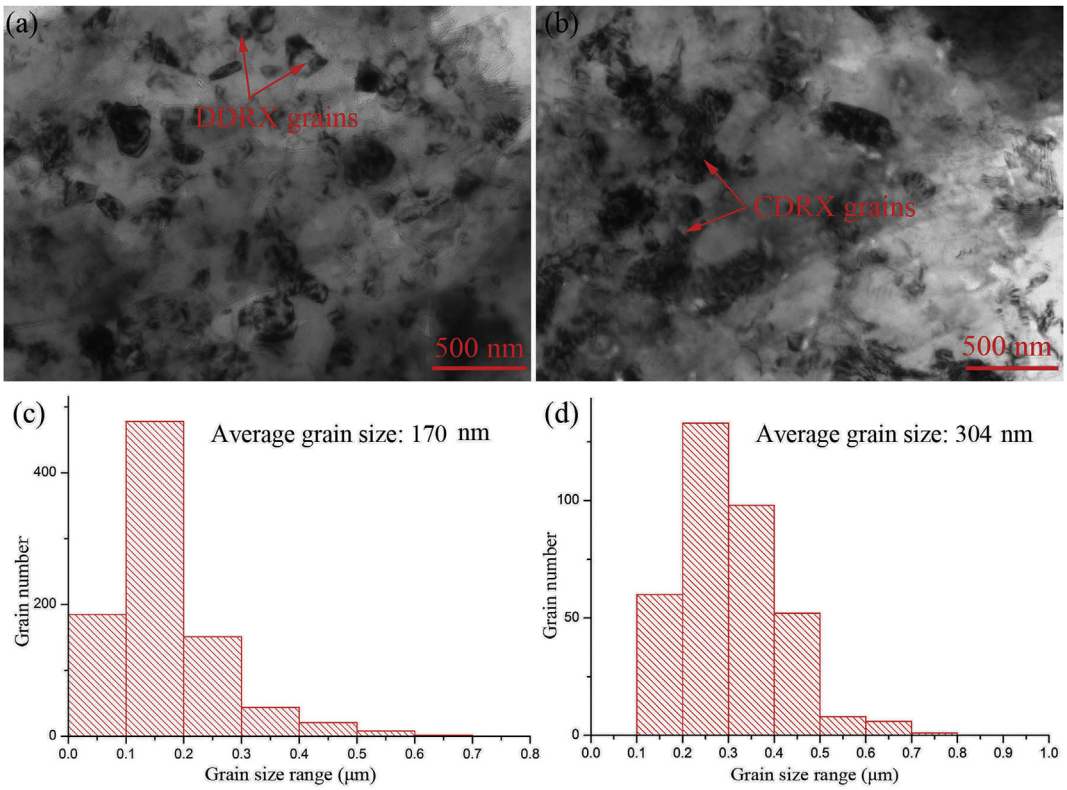

Fig. 3. TEM images and grain size distribution of 250 °C extruded LAJ932 alloy: (a) TEM image showing DDRX grains; (b) TEM image showing CDRX grains; (c) the grain size distribution of DDRX grains; (d) the grain size distribution of CDRX grains.

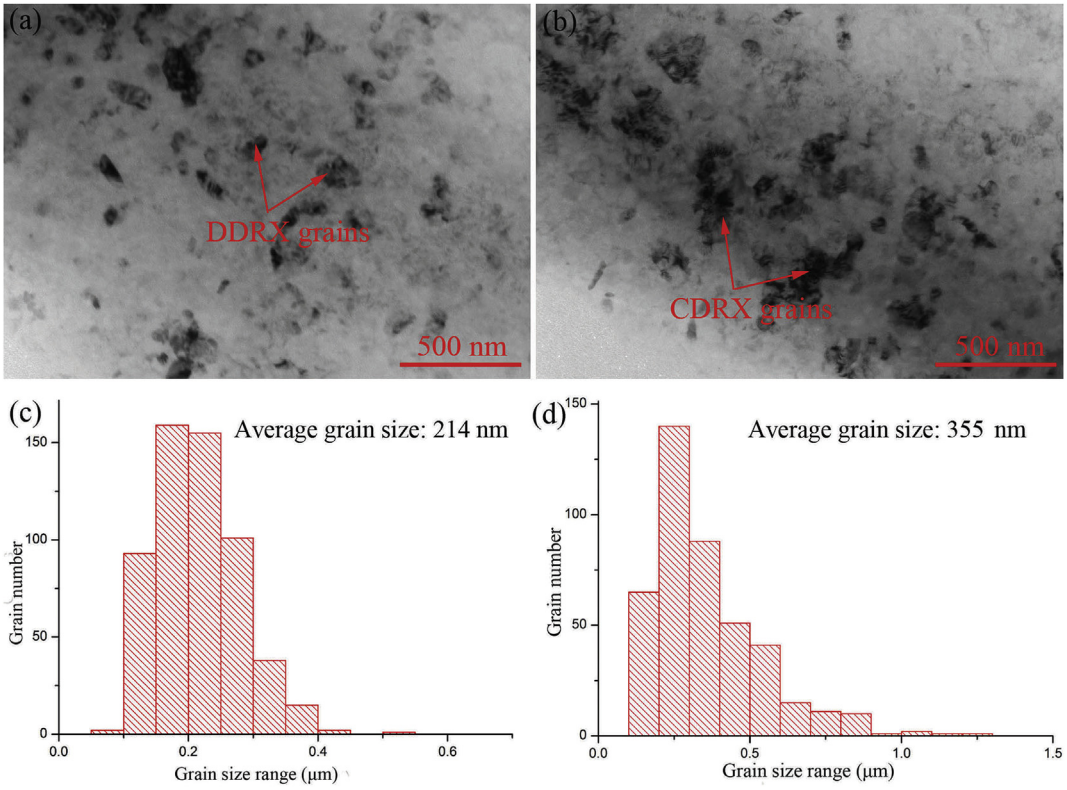

Fig. 4. TEM images and grain size distribution of 300 °C extruded LAJ932 alloy: (a) TEM image showing DDRX grains; (b) TEM image showing CDRX grains; (c) the grain size distribution of DDRX grains; (d) the grain size distribution of CDRX grains.

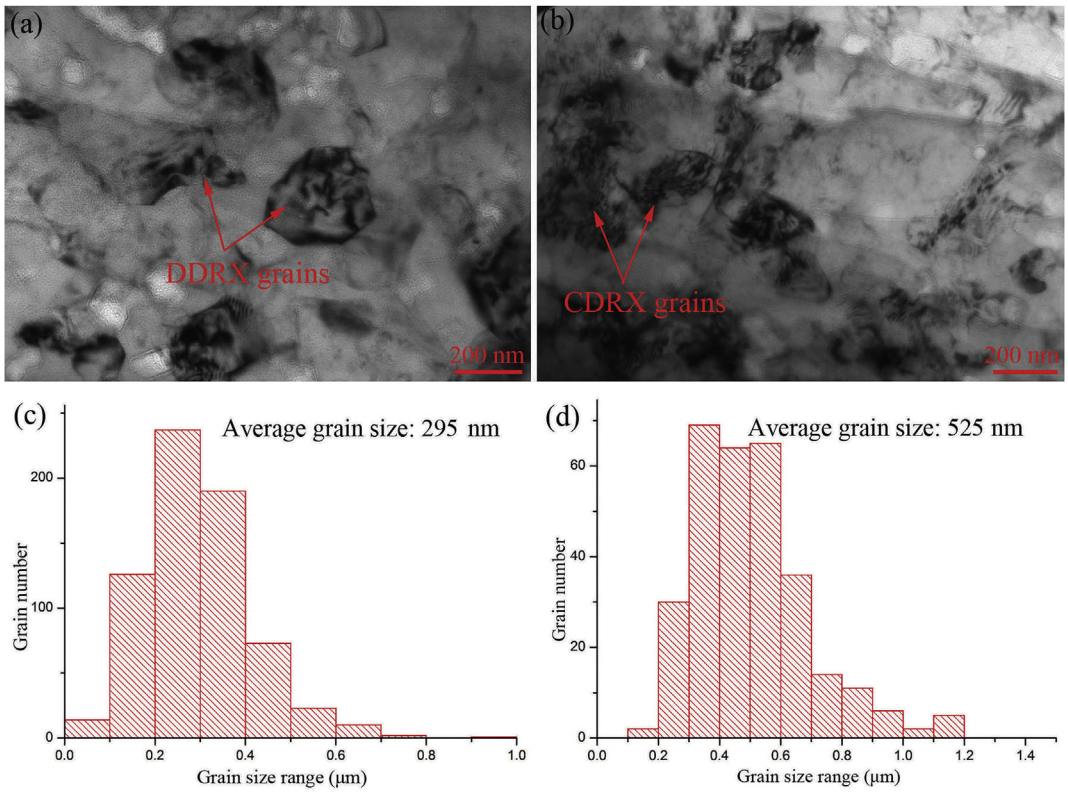

Fig. 5. TEM images and grain size distribution of 350 °C extruded LAJ932alloy: (a) TEM image showing DDRX grains; (b) TEM image showing CDRX grains; (c) the grain size distribution of DDRX grains; (d) the grain size distribution of CDRX grains.

distributed in 200–1000 nm. The OM and TEM results confirm that the grain size of the extruded Mg-9Li-3Al-2.5 Sr alloys increases with increasing extrusion temperature.

On the basis OM and TEM studies on grain morphology, it appears that when the extrusion temperature is 350 °C, some grains formed by discontinuous dynamic recrystallization (DDRX) are evident in the elongated α-Mg phase. Based on analysis of more than 60 TEM images, the amount of CDRX grains decreases with increasing extrusion temperature, indicating that a high extrusion temperature promotes the occurrence of DDRX. This result is consistent with the OM analysis. In order to distinguish the α-Mg phase from the β-Li phase and further investigate the differences between CDRX and DDRX grains, high-resolution TEM (HRTEM) was performed. Figs. 6 and 7 present HRTEM images of the 250 °C extruded alloy. Fig. 6(a) shows one CDRX grain with irregular grain boundary while Fig. 7(a) shows a DDRX grain with sharp and straight grain boundary; the insets in both figures are selected-area electron diffraction (SAED) patterns corresponding to the circled areas. Fig. 6(b) is the HRTEM image of the grain in Fig. 6(a) and (c) shows a set of lattice planes obtained by inverse Fourier transformation of Fig. 6(b). The interplanar spacing is measured as 0.241 nm, close to 0.245 nm, the interplanar spacing of $(1\bar{1}01)$ crystallographic planes of α-Mg phase. Thus the CDRX grain is confirmed as α-Mg phase. Fig. 7(b) is a HRTEM image of the grain in Fig. 7(a) and (c) shows a set of crystallographic planes obtained by inverse Fourier transformation of Fig. 7(b). The interplanar spacing is measured to be 0.247 nm, near to 0.248 nm, the interplanar spacing of $(0\bar{1}1)$ crystallographic planes of β-Li phase. Therefore, the DDRX grain is confirmed to be β-Li phase. Thus, these results further confirm that when the extrusion temperature is 250 °C, the microstructure evolution in the α-Mg phase during extrusion is governed by CDRX whereas DDRX occurs in the β-Li phase.

3.2. Mechanical properties of LAJ932 alloys bars with different extrusion temperatures

Fig. 8 shows the typical tensile stress-strain curves of LAJ932 alloy extruded at different temperatures with an extrusion ratio of 28. The tensile strength of the alloy extruded at 250 °C is 238 MPa with an elongation of 18.1%, while the tensile strength of the alloy extruded at 300 °C decreases to 223 MPa with an elongation of 19.7%. When the extruded temperature reaches 350 °C, the tensile strength of the extruded alloy decreases to 208 MPa, whereas the elongation increases to 21.6%. The strength of the extruded alloy decreases whereas the elongation increases with the increase of extrusion temperature. In related work, the strength of Mg-4Y-4Sm-0.5Zr was reported to decrease while the elongation increased with increasing extrusion temperature [22].

4. Discussion

4.1. Microstructure evolution during hot extrusion at different temperatures

The various microstructural characteristics of the α-Mg and the β-Li phases, as shown in Figs. 2–7, indicate that there are distinct mechanisms that likely govern microstructural refinement in the various phases during the hot extrusion process. Because of significant differences in physical properties such as melting point, ductility and crystal structure of the α-Mg and β-Li phases, the microstructure evolution in different phases during extrusion is anticipated to be different. Our previous research indicated that the microstructure evolution in the α-Mg phase is governed by CDRX whereas DDRX occurs in the β-Li phase during 260 °C extrusion with an extrusion ratio of 28 [18]. Usually, diffusion-controlled

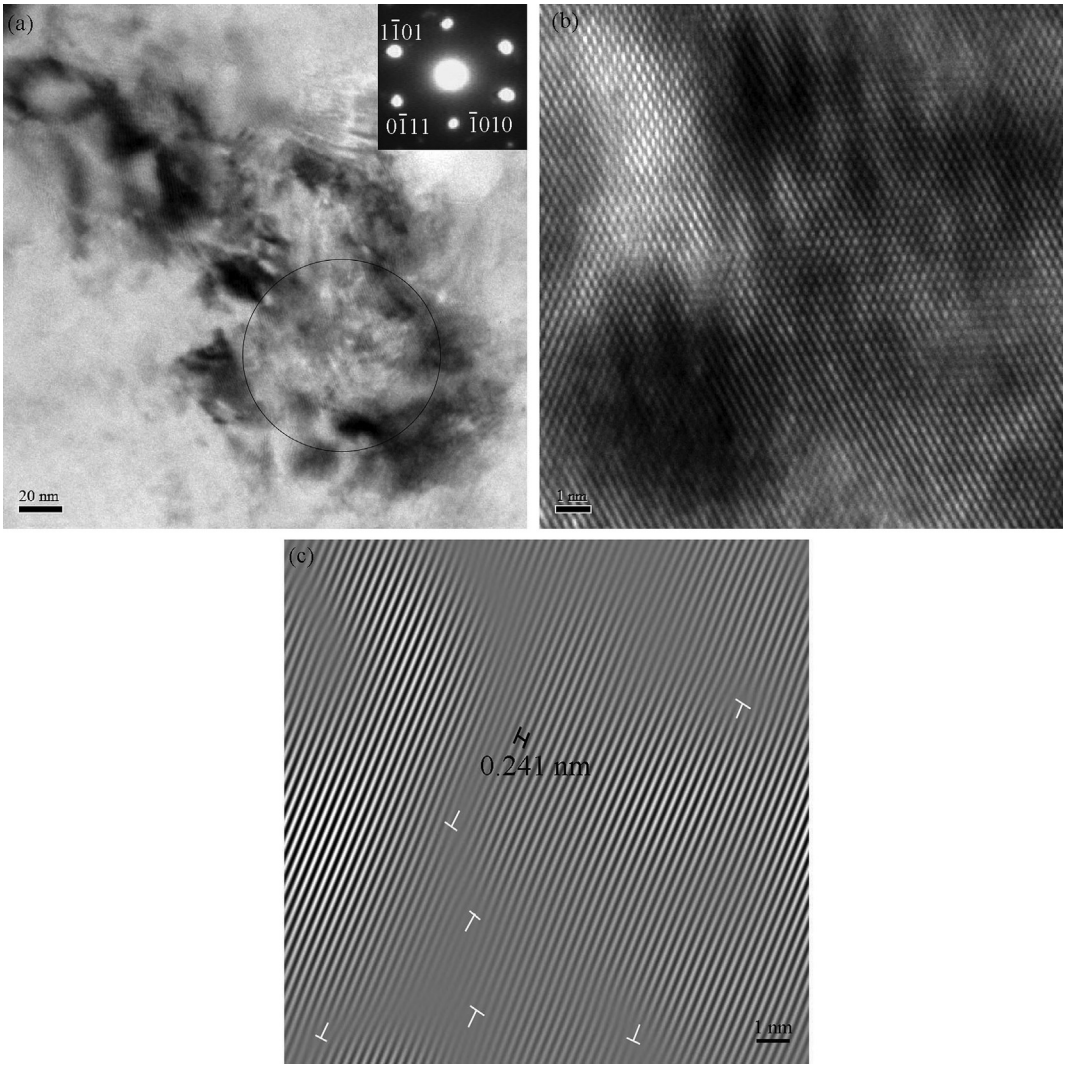

Fig. 6. TEM images of 250 °C extruded LAJ932 alloy: (a) TEM image showing a grain of α-Mg phase, where the inset is the SAED pattern corresponding to the circled area; (b) a lattice-fringe image of the grain in (a); (c) the (1–101) crystallographic planes obtained by inverse Fourier transformation of (b).

processes can be accelerated and the migration of grain boundaries can be facilitated at relatively high deformation temperatures. Thus DDRX is favored at relatively high temperatures. In contrast, CDRX is favored at relatively low temperatures. The influence of extrusion temperature on the mechanism of microstructure evolution in LAJ932 alloy is discussed as follows.

4.1.1. Microstructure evolution of α-Mg phase at different extrusion temperatures

The presence of irregular grain boundaries of primary α-Mg and eutectic α-Mg grains and high dislocation density in the grain interiors indicate that deformation-induced grain refinement has occurred in α-Mg phase [see Figs. 2, 3(b), 4(b), 5(b) and 6]. The microstructural features observed from OM and TEM for α-Mg phase at relatively low extrusion temperatures are consistent with the microstructural characteristics widely reported for CDRX [18,23,24]. At the early stage of CDRX, grains may be elongated along the deformation direction, which is consistent with our microstructure observations [see Fig. 2(b) (c) (d)]. CDRX is a strain-induced grain refinement process [25], which occurs in some severe plastic deformation techniques such as high pressure torsion and equal-channel angular pressing [21,26–28]. Strain is an important factor for CDRX. To understand the evolution of the strain field during extrusion, we completed simulation studies. The strain distribution during the extrusion at 300 °C with an extrusion ratio of 28 is shown in Fig. 9. The central region of the extruded specimen experiences the minimum strain, which is > 1.5, indicating that strain is significantly accumulated during extrusion. CDRX is one of the most important dynamic recrystallization (DRX) mechanisms in Mg and Mg alloys [29]. In related work H. Jazaeri et al. proposed that CDRX is facilitated by the presence of large second-phase particles and high strain [30,31]. In our study, the minimum strain in the extruded specimen experiences is > 1.5, due to the high extrusion ratio (28) used. The large strain promotes the occurrence of CDRX. In addition, the second-phase Al_4Sr particles likely promote the occurrence of CDRX in the α-Mg phase. On the basis of the above discussion we propose that CDRX is the dominant mechanism for microstructural refinement in both the primary α-Mg and eutectic α-Mg phase during extrusion at 250 and 300 °C with an extrusion ratio of 28.

Our results also show that the amount of CDRX grains decreases slightly with increasing extrusion temperature, suggesting that a high extrusion temperature promotes the occurrence of DDRX. When the extrusion temperature reaches 350 °C, some DDRX

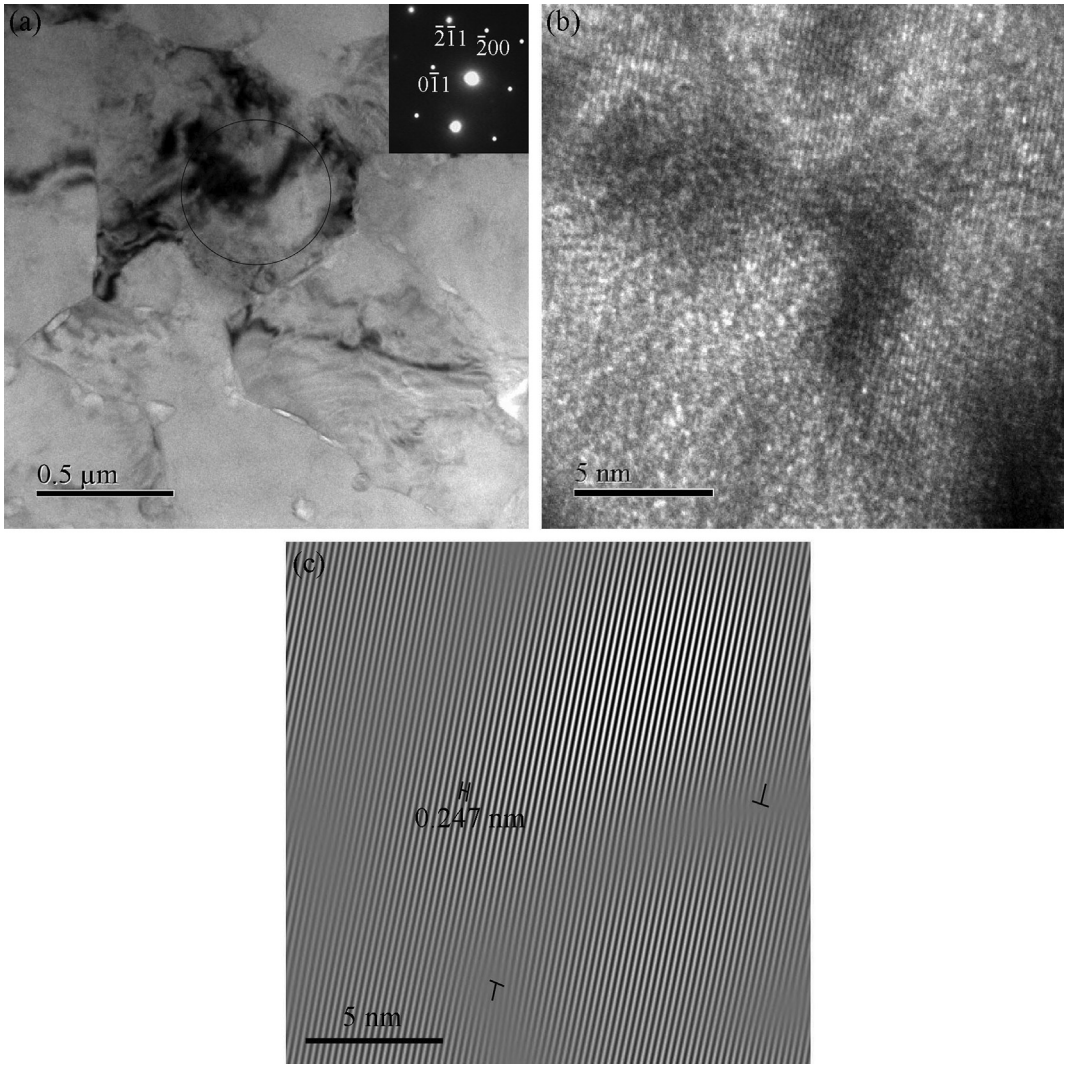

Fig. 7. TEM images of 250 °C extruded LAJ932 alloy: (a) TEM image showing a grain of β-Li phase, where the inset is the SAED pattern corresponding to the circled area; (b) a lattice-fringe image of the grain in (a); (c) the (0–11) crystallographic planes obtained by inverse Fourier transformation of (b).

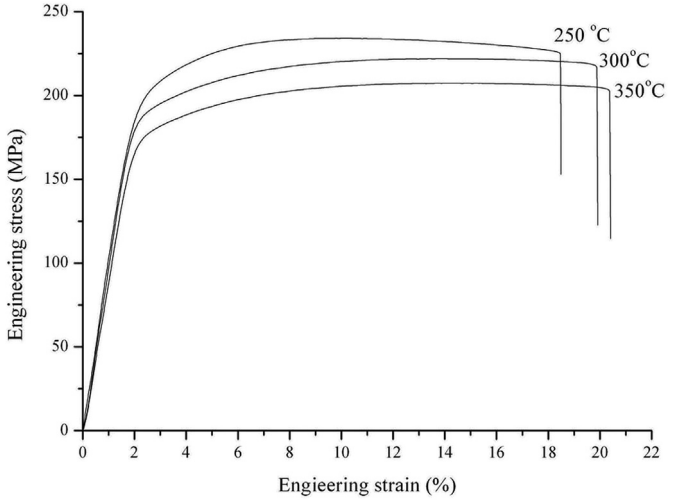

Fig. 8. Tensile stress-strain curve of extruded Mg-9Li-3Al-2.5Sr alloy with different extrusion temperatures.

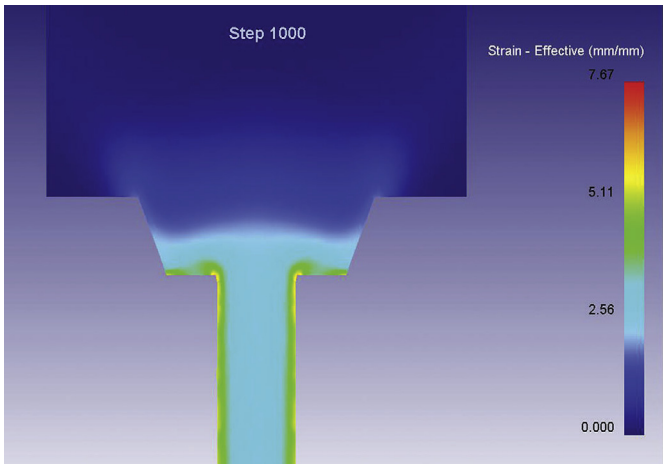

Fig. 9. The effective strain distribution during extrusion at 300 °C.

grains appear in α-Mg phase, as shown in Fig. 2(f). Thus although the microstructure evolution in α-Mg phase is governed by CDRX, a high extrusion temperature facilities some DDRX in the α-Mg phase. In related work, S. Gourdet has reported that CDRX mechanism is favored at lower temperature, and an increase in the deformation temperature will slow down CDRX, because dislocation recovery is enhanced with increasing temperature [24], which is consistent with our results. It has been reported in related work that DDRX is the primary grain refinement mechanism in Mg alloys during hot extrusion when the temperature exceeds 400 °C [32,33]. Based on the above discussion, it is inferred that DDRX is the main mechanism for the microstructure evolution in α-Mg phase if the extrusion temperature is sufficiently high.

4.1.2. Microstructure evolution of β-Li phase at different extrusion temperature

Typically, DDRX grains have sharp and straight grain boundaries and are relatively depleted of dislocations at grain interiors [18]. Sharp grain boundaries of the grains of β-Li phase and few dislocations inside the grains are typical characteristics of grains generated by DDRX [34,35]. The DDRX process starts with nucleation of new grains [36,37]. It then proceeds through growth of the nucleated new grains by migration of their grain boundaries, thereby leading to the consumption of the deformed matrix. A critical strain and a sufficiently high deformation temperature are required to initiate DDRX [38–40]. The β-Li phase with bcc structure is softer and has better ductility than α-Mg phase [18]. Therefore, plastic deformation occurs, first in the β-Li phase during extrusion, thereby making it easier for the β-Li phase to attain the critical strain required for DDRX. The effective strain distribution during extrusion, as shown in Fig. 9, indicates that the minimum strain in the extruded bars is > 1.5, which is large enough to meet the strain requirement of DDRX in β-Li phase. In addition, the melting point of the β-Li phase is relatively low (588 °C in the eutectic region), and thus the extrusion temperatures of 250, 300 and 350 °C are sufficiently high to meet the temperature requirement for DDRX. The presence of the α-Mg and the Al_4Sr phases facilitates DDRX in the β-Li phase [18,41,42]. With increasing extrusion temperature, DDRX is enhanced in the β-Li phase. In summary, we propose that DDRX is responsible for the formation of β-Li grains with sharp grain boundaries in the extruded alloys.

4.1.3. Microstructure evolution of intermetallic Al4Sr phase

Fig. 10 displays TEM and STEM images showing the intermetallic Al_4Sr phase in the as-cast and extruded LAJ932 alloys. Fig. 10(a) shows the continuous Al_4Sr network in the as-cast alloy. Fig. 10(b) displays the Al_4Sr particles in the extruded alloy. Note that bright contrast in a STEM image typically corresponds to a higher atomic number. Thus the bright areas in Fig. 10 (b) correspond to Al_4Sr. The continuous fish-bone like Al_4Sr phase in the as-cast alloy is fractured during the extrusion because Al_4Sr is brittle, and the distribution of Al_4Sr phase is improved significantly by extrusion. Thus approximately equiaxed Al_4Sr particles, in the size range of ~2–15 μm, are nearly homogeneously distributed in the extruded alloy. There is no evident influence of extrusion temperature on the distribution and characteristics of the Al_4Sr phase. Instead, it is anticipated that extrusion ratio has a significant influence on the size and distribution of the Al_4Sr phase because extrusion ratio influences the amount of deformation during extrusion.

4.1.4. Influence of extrusion temperatures on the grain size of LAJ932 alloy

The grains in the extruded LAJ932 alloys are significantly refined during hot extrusion due to continuous and discontinuous dynamic recrystallization as discussed above. However, the extrusion temperature critically influences grain size during extrusion. In our present work, both the average grain size of α-Mg phase and β-Li phase increases with increasing extrusion temperature as shown on Figs. 2–5. With increasing extrusion temperature, the kinetics for grain growth are enhanced [43,44]. G.S. Hu et al. [44] reported that grain growth occurred in Mg-6Zn-1Mn-4Sn-0.5Y alloy with increasing extrusion temperature. H. F. Sun et al. [45] showed that both dynamic recrystallized grain size and fraction increased with increasing deformation temperature. Similarly, a study by J. Peng et al. [32] indicated that the average grain size of Mg-2.0Zn-1.0Mn-0.2Ce alloys gradually increased with increasing extrusion temperature. Thereby, on the basis of our experiment results, and those from the published literature, we confirm that the grain size of the extruded alloy increases with the increasing extrusion temperature.

4.2. Influence of extrusion temperature on the mechanical properties of LAJ932 alloy rods

Extrusion temperature critically influences grain size and microstructure evolution which in term governs the mechanical behavior of the alloys. A multimodal microstructure was formed in the test alloys during hot extrusion. In principle such a multimodal microstructure should influence the mechanical behavior of the

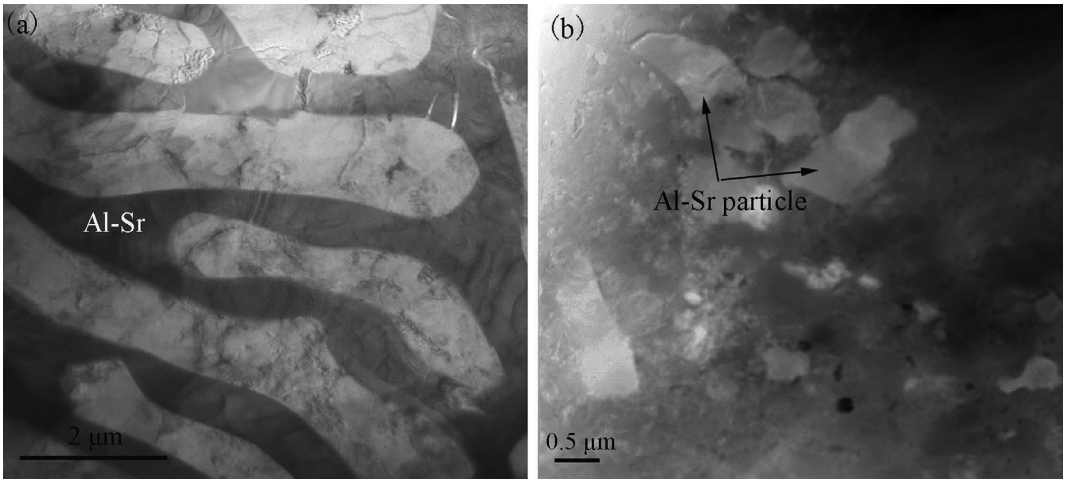

Fig. 10. TEM and STEM images showing Al_4Sr phase in LAJ932 alloy: (a) TEM image showing the continuous Al_4Sr phase in the as-cast alloys; (b) STEM image showing the Al_4Sr particles in the 250 °C extruded alloy.

alloys. In such microstructure it is generally found that the coarse grains benefit ductility whereas the fine grains contribute to an improvement in strength. In related studies, J.H. He, L. Jin et al. [46] investigated the influence of bimodal grain size distributions on the mechanical properties of Mg-8Gd-3Y-0.5Zr alloy. Their results show that the bimodal grain size distribution has no significant effect on the strength but a notable influence on the ductility. The improvement of strength of Mg-8Gd-3Y-0.5Zr alloy is still attributed to the grain refinement whereas the elongation to failure increases at first and then decreases with an increase in coarse-grain volume fraction. Quantitative analysis of the influence of the multimodal microstructure (the relatively wide grain size distribution) on the mechanical properties requires very detailed and dedicated study and therefore is not performed in the present work. The influence of extrusion temperature on the mechanical properties is analyzed considering the following three factors.

4.2.1. Grain boundary strengthening

The microstructural studies of extruded LAJ932 alloys discussed above reveal that the grain size increases with increasing extrusion temperature. On the basis of Hall-Petch relationship,

$$\Delta\sigma_{bs} = kd^{-1/2} \quad (1)$$

where k is a constant (= 0.28 MNm-3/2 for Mg [47]) and d is the average grain size, we can estimate the contributions from grain boundary strengthening mechanism. According to Equation (1), grain size has significant influence on the strength. If we consider the primary α-Mg phase as an example, the average size of primary α-Mg phase is ~12 μm when the extrusion temperature is 250 °C while the value reaches to 16 and ~23 μm with the temperature increasing to 300 and 350 °C, respectively. The calculated strength of primary α-Mg in the alloy extruded at 250 °C due to grain boundaries strengthening is ~81 MPa whereas the value decreases to ~70 MPa and ~58 MPa with the temperature increasing to 300 and 350 °C, respectively. Thus, the strength of the primary α-Mg phase is reduced to ~11 MPa and ~23 MPa respectively due to grain growth with increasing extrusion temperature.

4.2.2. Dislocation strengthening

A low deformation temperature promotes the CDRX process while a high deformation temperature is beneficial to DDRX. Thus the amount of DDRX grains increases with the increasing extrusion temperature. One typical characteristic of CDRX grains is the high dislocation density inside the grain interiors, whereas there are few dislocations in the DDRX grains [18,42]. Thus the dislocation density in the extruded alloy with high extrusion temperature is anticipated to be lower than that in the alloy with lower extrusion temperature. Based on the Taylor equation,

$$\sigma_{ds} = M\alpha Gb\rho^{1/2} \quad (2)$$

where M is Taylor factor, α is a constant, G is the shear modulus, b is the Burgers vector, and ρ is the dislocation density, the contribution to strength that derives from dislocations can be estimated. Based on Equation (2), it can be confirmed that high dislocation density will indeed contribute to the improvement in strength.

4.2.3. Influence of texture

Texture usually has a significant effect on the mechanical behavior of extruded Mg alloys. Typically, Mg alloys with an hcp structure exhibit strong basal plane texture after hot axisymmetric extrusion with the basal plane parallel to the extrusion axis [42,48]. Basal texture hinders the activation of basal dislocations, which is beneficial to an improvement of strength, but not good for the ductility. In related work, Chao Xu [49] et al. reported that Mg-7.5Gd-2.5Y-3.5Zn-0.9Ca-0.4Zr (wt%) alloy extruded at 400 °C exhibit strong basal fiber texture. With the extrusion temperature increasing to 450 °C and 500 °C, completed dynamic recrystallization occurs in the test alloys, leading to weak basal fiber texture, which benefits ductility. In this study, CDRX governs the microstructure evolution of α-Mg phase at the extrusion temperature of 250 °C, which likely leads to the formation of basal texture, which enhances strength but degrades ductility. With increasing extrusion temperature to 300 °C and 350 °C, DDRX occurs in α-Mg phase to some extent and weak basal fiber texture, which enhances ductility. Because DDRX is the primary microstructure evolution mechanism in β-Li phase, we argue that the texture in β-Li will have very limited influence on mechanical response for the range of extrusion temperatures studied herein.

As discussed above, the strength of the extruded alloy should decrease with the increasing extrusion temperature if only considering grain boundary strengthening dislocation strengthening and the influence of texture [50–53]. In addition, the elongation of the extruded alloy increases with the increasing extrusion temperature, which can be rationalized on the basis of several factors. The average grain size of the extruded alloy increases slightly with the increasing extrusion temperature. Usually, larger grains have a greater capability for dislocation storage and accumulation [42], which benefits ductility. Furthermore, as discussed above, the dislocation density is lower in the alloy extruded at higher temperature. Grains with a lower dislocation density can provide more space for dislocation accumulation during tensile testing, which results in larger strain-hardening [21,42]. Thus the elongation of the extruded alloy increases with the increasing extrusion temperature.

5. Conclusions

In this work, Mg-Li-Al-Sr alloys rods extruded at different temperatures were prepared. The microstructure and mechanical response of extruded Mg-Li-Al-Sr alloys rods were systematically investigated. The influence of extrusion temperature on the tensile mechanical behavior of extruded Mg-Li-Al-Sr alloys rods was discussed. The following conclusions can be drawn.

1) Both the as-cast and extruded LAJ932 alloys contain α-Mg phase, β-Li phase and Al_4Sr phase. The grain size of the extruded alloys increases with the increase of extrusion temperature. The original continuous fish-bone like Al_4Sr phase is broken into approximately equiaxed Al_4Sr particles with size of ~2–15 μm by extrusion. There is no evident influence of extrusion temperature on the Al_4Sr phase in the extruded alloys bars.
2) The microstructure evolution during extrusion is governed by CDRX in the α-Mg phase whereas DDRX in the β-Li phase when the extrusion temperature is below to 300 °C. With increasing extrusion temperature to 350 °C, DDRX occurs in α-Mg phase to some extent.
3) The strength of extruded LAJ932 alloys bars decreases whereas the ductility increases with the increasing extrusion temperature. The alloy extruded at 350 °C possesses the largest elongation of 21.6% with a tensile strength of 208 MPa while the 250 °C extruded alloy has the highest tensile strength of 238 MPa with an elongation of 18.1%.

Acknowledgements

The authors would like to acknowledge financial support by the National Natural Science Foundation (Project No. 51601024), the National Key Research and Development Program of China (Project

No. 2016YFB0700403 & Project No. 2016YFB0301100), the Chongqing Research Program of Basic Research and Frontier Technology (Project No. cstc2016jcyjA0418), the Fundamental Research Funds for the Central Universities (Project No. 106112016CDJXZ138811) and the support of the 111 Project (Project No. B16007) by the Ministry of Education and the State Administration of Foreign Experts Affairs of China. The authors (Yan Yang, Enrique J. Lavernia) are also grateful to the financial support from National Science Foundation (Project No. CMMI-1729829).

References

[1] J. Shao, Z. Chen, T. Chen, Z. Hu, X. Zhou, C. Liu, J. Magn. Alloy. 4 (2016) 83–88.
[2] Y. Yang, X.D. Peng, F.J. Ren, H.M. Wen, J.F. Su, W.D. Xie, J. Mater. Sci. Technol. 32 (2016) 1289–1296.
[3] S.A. Askariani, S.M.H. Pishbin, J. Alloys Compd. 688 (2016) 1058–1065.
[4] T.C. Xu, X.D. Peng, J. Qin, Y.F. Chen, Y. Yang, G.B. Wei, J. Alloy. Compd. 639 (2015) 79–88.
[5] R. Wu, Y. Yan, G. Wang, L.E. Murr, W. Han, Z. Zhang, M. Zhang, Int. Mater. Rev. 60 (2015) 65–100.
[6] S. You, Y. Huang, K.U. Kainer, N. Hort, J. Magn. Alloy. 5 (2017) 239–253.
[7] D.K. Xu, B.J. Wang, C.Q. Li, T.T. Zu, E.H. Han, Mater. Des. 69 (2015) 124–129.
[8] X.J. Wang,D.K. Xu, R.Z. Wu, X.B. Chen, Q.M.Peng, L.Jin, Y.C.Xin, Z.Q.Zhang, Y.Liu, X.H.Cheng, G.Chen, K.K.Deng, H.Y.Wang, J. Mater. Sci. Technol. https://doi.org/10.1016/j.jmst.2017.07.019.
[9] M.J. Phasha, P.E. Ngoepe, H.R. Chauke, D.G. Pettifor, D. Nguyen-Mann, Intermetallics 18 (2010) 2083–2089.
[10] R. Mahmudi, M. Shalbafi, M. Karami, A.R. Geranmayeh, Mater. Des. 75 (2015) 184–190.
[11] G.Y. Sha, X.G. Sun, T. Liu, Y.H. Zhu, T. Yu, J. Mater. Sci. Technol. 27 (2011) 753–758.
[12] X. Meng, R. Wu, M. Zhang, L. Wu, C. Cui, J. Alloys Compd. 486 (2009) 722–725.
[13] T. Wang, M. Zhang, R. Wu, Mater. Lett. 62 (2008) 1846–1848.
[14] T. Chang, J. Wang, C. Chu, S. Lee, Mater. Lett. 60 (2006) 3272–3276.
[15] X. Liu, H. Zhan, S. Gu, Z. Qu, R. Wu, M. Zhang, Mater. Sci. Eng. A. 528 (2011) 6157–6162.
[16] Y. Zhang, J. Zhang, G. Wu, W. Liu, L. Zhang, W. Ding, Mater. Des. 66 (2015) 162–168.
[17] H. Dong, F. Pan, B. Jiang, Y. Zeng, Mater. Des. 57 (2014) 121–127.
[18] Y. Yang, X. Peng, H. Wen, B. Zheng, Y. Zhou, W. Xie, E.J. Lavernia, Mater Trans A 44 (2013) 1101–1113.
[19] Y. Yang, X. Peng, W. Xie, Q. Wei, G. Chen, Z. Su, Mater. Sci. Forum 686 (2011) 84–89.
[20] D. Tang, Q. Zhang, D. Li, Y. Peng, J. Mater. Process. Technol. 214 (2014) 2777–2783.
[21] H.M. Wen, Y.H. Zhao, T.D. Topping, D. Ashford, R.B. Figueiredo, C. Xu, T.G. Langdon, E.J. Lavernia, Adv. Eng. Mater. 14 (2012) 185–194.
[22] D. Li, Q. Wang, W. Ding, Trans. Nonferrous Metals Soc. China 20 (2010) 1311–1315.
[23] S. Gourdet, F. Montheillet, Mater. Sci. Eng. A. 283 (2000) 274–288.
[24] S. Gourdet, F. Montheillet, Acta Mater. 51 (2003) 2685–2699.
[25] T. Sakai, H. Miura, A. Goloborodko, O. Sitdikov, Acta Mater. 57 (2009) 153–162.
[26] V.M. Segal, Mater. Sci. Eng. A. 271 (1999) 322–333.
[27] T. Nakata, T. Mezaki, C. Xu, K. Oh-ishi, K. Shimizu, S. Hanaki, S. Kamado, J. Alloys Compd. 648 (2015) 428–437.
[28] H. Miura, M. Ito, X. Yang, J.J. Jonas, Mater. Sci. Eng. A. 538 (2012) 63–68.
[29] J. Li, D. Lin, D. Mao, X. Zeng, B. Chen, W. Ding, Mater. Sci. Eng. A. 423 (2006) 247–252.
[30] H. Jazaeri, F.J. Humphreys, Acta Mater. 52 (2004) 3239–3250.
[31] H. Jazaeri, F.J. Humphreys, Acta Mater. 52 (2004) 3251–3262.
[32] J. Peng, L. Zhong, Y. Wang, Y. Lu, F. Pan, Mater. Des. 87 (2015) 914–919.
[33] S. Aliakbari Sani, G.R. Ebrahimi, A.R. Kiani Rashid, J. Magn. Alloy. 4 (2016) 104–114.
[34] K. Ahn, H. Lee, J. Yoon, Mater. Sci. Eng. A. 651 (2016) 1010–1017.
[35] H.C. Xiao, S.N. Jiang, B. Tang, W.H. Hao, Y.H. Gao, Z.Y. Chen, C.M. Liu, Mater. Sci. Eng. A. 628 (2015) 311–318.
[36] N. Dudova, A. Belyakov, T. Sakai, R. Kaibyshev, Acta Mater. 58 (2010) 3624–3632.
[37] H. Hallberg, M. Wallin, M. Ristinmaa, Comput. Mater. Sci. 49 (2010) 25–34.
[38] G.Z. Quan, Y. Shi, Y.X. Wang, B.S. Kang, T.W. Ku, W.J. Song, Mater. Sci. Eng. A. 528 (2011) 8051–8059.
[39] C.X. Yue, L.W. Zhang, S.I. Liao, J.B. Pei, H.J. Gao, Y.W. Jia, X.J. Lian, Mater. Sci. Eng. A. 499 (2009) 177–181.
[40] G.L. Ji, F.G. Li, Q.H. Li, H.Q. Li, Z. Li, Mater. Sci. Eng. A. 527 (2010) 2350–2355.
[41] Y. Yang, X. Peng, W. Xie, G. Wei, F. Xu, Q. Wei, Rare Metal Mater. Eng. 43 (2014) 1281–1285.
[42] Y. Yang, X. Peng, H. Wen, G. Wei, W. Xie, E.J. Lavernia, Mater. Sci. Eng. A. 611 (2014) 1–8.
[43] H. Wang, J. Rong, G. Liu, M. Zha, C. Wang, D. Luo, Q. Jiang, Mater. Sci. Eng. A. 698 (2017) 249–255.
[44] G.S. Hu, D.F. Zhang, T. Tang, L.Y. Jiang, F.S. Pan, Rare Metal Mater. Eng. 45 (2016) 1111–1116.
[45] H.F. Sun, C.J. Li, W.B. Fang, J. Mater. Process. Technol. 229 (2016) 633–640.
[46] J.H. He, L. Jin, F.H. Wang, S. Dong, J. Dong, J. Magn. Alloy. 5 (2017) 423–429.
[47] W.J. Kim, I.K. Moon, S.H. Han, Mater. Sci. Eng., A 538 (2012) 374–385.
[48] Q. Liu, X. Zhou, H. Zhou, X. Fan, K. Liu, J. Magn. Alloy. 5 (2017) 202–209.
[49] C. Xu, T. Nakata, X.G. Qiao, H.S. Jiang, W.T. Sun, Y.C. Chi, M.Y. Zheng, S. Kamado, Mater. Sci. Eng. A. 685 (2017) 159–167.
[50] B. Liu, D. Raabe, P. Eisenlohr, F. Roters, A. Arsenlis, G. Hommes, Acta Mater. 59 (2011) 7125–7134.
[51] Y. Li, Y.H. Zhao, V. Ortalan, W. Liu, Z.H. Zhang, R.G. Vogt, N.D. Browning, E.J. Lavernia, J.M. Schoenung, Mater. Sci. Eng. A. 527 (2009) 305–316.
[52] H. Wen, T.D. Topping, D. Isheim, D.N. Seidman, E.J. Laverni, Acta Mater. 61 (2013) 2769–2782.
[53] K. Ma, H. Wen, T. Hu, T.D. Topping, D. Isheim, D.N. Seidman, E.J. Laverniaa, J.M. Schoenung, Acta Mater. 62 (2014) 141–155.